Differential abundance analysis of Procyon and θ Sculptoris: Comparison with abundance patterns of solar-like pairs

C. R. Cowley*[1] | K. Yüce[2] | D. J. Bord[3]

[1]Department of Astronomy, University of Michigan, Ann Arbor, 1085 S. University, Michigan 48109-1107, USA

[2]Department of Astronomy and Space Sciences, Faculty of Science, University of Ankara, Ankara, TR-06100, Turkey

[3]Department of Natural Sciences, University of Michigan–Dearborn, 4901 Evergreen Road, Dearborn, MI 48128, USA

Correspondence
*C. R. Cowley Email: cowley@umich.edu

The precision differential abundance (PDA) technique is applied to the mid-F stars Procyon and θ Scl using spectra from the ESO UVESPOP library. We relate PDA patterns to endogenous processes related to condensation or to exogenous processes connected to Galactic chemical evolution (GCE). We employ one-dimensional LTE models, but emphasize the use of weaker lines (≤ 20 mÅ) than are typically used in such studies. We compare our results with PDAs of solar-type stars. Abundances and PDAs are determined for 28 elements: C, N, O, Na, Mg, Al, Si, S, Ca, Sc, Ti, V, Cr, Mn, Fe, Co, Ni, Cu, Zn, Y, Zr, Ba, La, Ce, Nd, Sm, Eu, and Gd. A plot of PDAs (θ Scl minus Procyon) vs. Z shows a highly significant correlation. Moreover, local substructure of the plot for the elements Ca-Zn and neutron-addition elements is similar to that which can be found for solar twins. Our PDA vs. Z plot structural similarity to plots that can be made from the extensive work of Bedell et al. (2018). That PDA structure and substructure is clearly a function of age.

KEYWORDS:
stars:abundances, stars:solar-type, stars:individual: Procyon, stars:individual:θ Scl

Lawrence Aller (1963) discussed the differential abundance method used by mid-20th century astronomers. In it, one characterized stellar atmospheres by single, mean values of temperature and pressure. The method allowed one to avoid the use of gf-values which were often highly uncertain. This technique has been revised and updated in connection with analyses of solar twins (Melendez, et al. 2009; Nissen & Gustafsson 2018). In the modern technique, one determines basic stellar parameters and abundances from individual lines in the standard way (Gray 2005), using model atmospheres, equivalent widths and/or spectral synthesis. Differential abundances are then calculated from corresponding line pairs in the twin stars.

A primary advantage of the historical work, near independence from gf-values, is retained. The pairs are chosen to have identical or nearly identical spectral types, and presumably closely comparable structures and abundances to be "twins."

The precision of the method has revealed significant differences which may arise as a result of star formation and Galactic chemical evolution (Bedell et al. 2018, henceforth, BD18).

1 | THE STARS AND THEIR SPECTRA

Ramirez, Meléndez & Asplund (2014, henceforth RAM14) carried out an extensive study of mid and late F-star pairs. They noted that the thinness of the F-star convection zones relative to those of the well-explored solar twins would make it easier to detect abundance anomalies due, for example, to planet formation. Rather than making comparisons with the Sun, they defined and had stars from within their sample.

In the current work, we choose to compare two similar mid-F stars, slightly hotter than those of the RAM14 sample. Procyon (HD 61421) is a well-studied binary, consisting of an F5 IV-V and a white dwarf. Its composition is generally considered "indistinguishable from solar" (Liebert et al. 2013). The star,

θ Scl (HD 739), is a single-lined binary (Fuhrmann & Chini 2012, Fuhrmann et al. 2017). Its spectral type is F5 V. Contributions from the companions of either star are neglected in this study, although Procyon could be affected by pollution from its companion.

Numerous studies have given abundances for Procyon (Liebert et al. 2013). Selective abundances for θ Scl are given by Fuhrmann et al. (2017) and Battistini & Bensby (2015). The former work is not differential, while latter compares F-stars with the Sun and therefore is distinct from twin studies, which usually involve stars with effective temperatures differing by some 100K or less.

Procyon and θ Scl are in the ESO UVESPOP library (Bagnulo, et al. 2003) which provides the high-quality spectra suitable to apply the differential-twin abundance method in the F-star domain. The spectra are of comparable quality to those used used to analyze solar twins (S/N 300-700, RP 80,000).

2 | SELECTION AND MEASUREMENT OF THE LINE SPECTRA

Lines were chosen from lists from Bedell et al. (2014) and Nissen (2015), but largely from the Procyon identification list published on Cowley's web site [1]. We selected lines with no obvious blends for which the measured and Ritz wavelengths were $\leq$ 0.03Å apart. Emphasis was given to weak ($\leq$ 20 mÅ) lines (see Sec. 4). Each line was then synthesized to discern the contribution of possible blends. The decision to use a particular line was aided by a synthesis with most of the broadening turned off, e.g. no turbulent or instrumental broadening. Additional useful information came from a synthesis with the contribution from the line in question turned off.

We chose to measure equivalent widths with the automatic routine ARES (Sousa et al. 2015). The code was downloaded from S. G. Sousa's web site [2] and installed under LINUX. Our own measurements, especially those of KY, using IRAF's Gaussian fits, agreed well with those of ARES. We decided that automatic measurements would remove any influence of a personal equation from the results if the input parameters to ARES are the same for both stars.

3 | MODELS AND SOFTWARE

Atlas9 models with solar abundances were used by both CRC and KY. Solar abundances are from Asplund et al. (2009) with updates by Scott et al. (2015), and Grevesse et al. (2015). To obtain abundances from an equivalent width, KY used

WIDTH9, while CRC fit Voigt profiles (cf. Cowley et al. 2014, and references therein). We used a set of 22 Fe I and 33 Fe II lines. The equivalent widths of these iron lines ranged from 3 to 90 mÅ. The mean difference of our measurements of log(W), CRC−KY, was 0.0031 dex. These lines were used to determine the microturbulent velocity and to ensure that the abundances were independent of excitation potential.

The standard method of deriving the microturbulence is to require that the stronger lines agree in abundance with the weakest ones. However, this removes virtually all abundance information from the strongest lines. Because of this, we have based our final model parameters on 12 Fe I lines and 13 Fe II lines with equivalent widths $\lesssim$ 20mÅ (Tab. 1). Our calculations used LTE and 1-dimensional models as is still common in differential analyses (Nissen & Gustafsson 2018).

In order to choose values of T_{eff} and log(g) for abundance calculations, four or five models were calculated, based on initial estimates from the literature and spectral types. Fe I and II abundances (Ab) were calculated for these models. They were assumed to obey a linear relation:

$$Ab = a \cdot T_{\mathrm{eff}} + b \cdot \log(g) + c. \tag{1}$$

The coefficients were determined separately by least squares for the reduced set of Fe I and Fe II lines (cf. Tab. 1) and then the right-hand sides of Eq. 1 were set equal to each other. This gives a linear relation between T_{eff} and log(g), or a line on a Kiel Diagram (Hunger 1955). This relation is also a function of the lines chosen and their gf-values (see Sec. 4).

To fix our final T_{eff} and log(g), we used Strömgren (Smalley 2014) and Geneva (Künzli et al. 1997) photometry, synthesis and comparison of the Balmer-line profiles, as well as the requirement that Fe I and Fe II yield the same abundance. Our adopted model for Procyon has T_{eff} = 6550K and log(g) = 3.9, with $v \cdot \sin(i)$ = 3.0 km/sec and a microturbulence of 2.0 km/sec. For θ Scl, these values were 6525K, 4.3, 3.0 km/sec, and 1.7 km/sec. A possible contribution from macroturbulence is included in our values of $v \cdot \sin(i)$, which were found by spectrum synthesis. These figures are in agreement with values in the literature (cf. Allende Prieto et al. 2002; Fuhrmann & Chini 2012). Uncertainties in the models and their effect on our results are discussed in Sect. 5.

4 | LINES AND TRANSITION PROBABILITIES: ABUNDANCES

4.1 | Iron

The use of very weak lines has advantages and disadvantages. Weak lines cannot be measured as accurately as stronger ones. In our experience, this is true both for lines measured "by eye" as well at those measured by ARES. Additionally, reliable

---

[1] http://www-personal.umich.edu/~cowley/procyon/wlid.html
[2] http://www.astro.up.pt/~sousasag/ares/

TABLE 1 Adopted weak Fe I and Fe II lines

	Fe I			Fe II	
$\lambda(\text{Å})$	$\log(gf)$	Desc.	$\lambda(\text{Å})$	$\log(gf)$	Desc.
4808.148	-2.668	sol	4720.139	-4.570	sol
5295.312	-1.557	sol	4833.192	-4.621	sol
5386.333	-1.730	sol	4953.980	-2.680	sol
5441.339	-1.588	sol	5000.730	-4.733	sol
5491.832	-2.188	C+	5161.175	-4.203	sol
5696.089	-1.720	C+	5427.816	-1.545	sol
5855.076	-1.478	C+	5525.117	-3.970	C
6226.734	-2.098	sol	5591.360	-4.527	sol
6271.278	-2.703	C+	6113.319	-4.078	sol
6725.356	-2.212	sol	6179.390	-2.797	sol
6733.150	-1.456	sol	6239.357	-4.812	sol
6837.006	-1.687	B	6248.907	-2.427	sol
			6446.407	-1.960	V3

oscillator strengths are more difficult to find for weak features (see below). On the other hand, curve of growth effects (e.g., microturbulence and hyperfine structure) are reduced by the use of weak lines. In Cowley & Yüce (2019), we found that for a typical Fe I line with an equivalent width of 15.2 mÅ, the saturation effect weakened the line by 17%. Although with differential methods, oscillator strengths cancel, this is only true for very weak lines and for lines where the saturation effects associated with turbulence and damping are taken precisely into account.

Oscillator strengths with NIST (Kramida et al. 2019) ratings of C or better were available for a few of our weak lines. Results using values from BRASS (Laverick et al. 2019) or VALD3 (V3, Ryabchikova et al. 2015) for the remaining lines led to results with wide scatter. For those lines, we ultimately chose solar gf-values derived in this work from ARES measurements using the Kurucz solar flux atlas (Kurucz et al. 1984). The Fe lines and adopted $\log(gf)$ values are shown in Tab. 1. The column labeled "Desc" gives the NIST accuracy rating or "sol," to indicate that solar gf-values were adopted. Of 12 the Fe I lines in Tab. 1, nine overlap with Bedell et al (2014). For these lines the agreement is excellent, especially for five of the lines for which solar values were derived. None of our Fe II lines overlapped with Bedell et al (2014).

4.2 | Other elements

In order to select lines for analysis, ARES was given a list of all lines from the Procyon identification list which had a single attribute whose wavelength differed by $\leq 0.03\text{Å}$. We then chose lines, with a few exceptions, having equivalent widths ≤ 20 mÅ. Of the 174 lines used for abundances, eight have

equivalent widths ≥ 20 mÅ. The largest of these was Eu II with 45.5 mÅ in Procyon. Generally, hyperfine structure was not taken into account for our weak lines, but for this line in Eu II it was approximately taken into account using the data of VALD3.

The regions near all of these lines were synthesized, as described for the iron lines. While virtually all of the lines had small blends, lines were retained unless the blends were estimated to contribute 10% or more to equivalent widths.

All of the lines judged suitable for analysis in the Procyon spectrum were adopted for θ Scl, provided there was an ARES measurement. In a few cases, lines measured by ARES for Procyon were not measured in θ Scl. Usually such lines were discarded from the analysis, but rarely, the lines were remeasured by CRC. Such measurements intercompare very well for weak lines with KY's IRAF values. The lines in question are: Nd II 5092.77, 5092.81 and Gd II 4316.04.

We consulted the bibliographic reference data of NIST (Kramida et al. 2019) to select the most recently determined oscillator strengths. Where practical, we cite original work rather than compilations (see Column 9 in Tab. 2).

Derived abundances are given in Tab. 2. The abundances are for $\log(El/N_{\text{tot}}) = \log(El/H) - 0.036$. The Difference column is for (θ Scl minus Procyon). The error of the differences is calculated for the N individual line pairs for each spectrum. Data for individual lines are given in Tab. 3.

5 | ERRORS

We have listed standard errors in Tab. 2, which are smaller by $\sqrt{N}$ than standard deviations, which can readily be obtained using Tab. 2. In general, while standard errors are technically correct, standard deviations often give a more realistic estimate of the uncertainties because statistical analysis does not account for systematic errors. The present differential technique should eliminate many systematic errors, however.

The average standard error of our differential abundances (Column 8 of Tab. 2) is 0.0294 dex. Overall, we have not reached the level of accuracy, 0.01 dex, of the solar twin studies (e.g. Meléndez et al. 2009; Nissen 2015), although for a few species, including Fe I and II, our standard errors are of the order of 0.01 dex.

Uncertainties in the model parameters introduce some error. Cowley & Yüce (2019, see Series 3 slide 3) gave results of a differential analysis for two sets of parameters describing Procyon and θ Scl. One set of results for Fe I and Fe II used the current parameters ($T_{\text{eff}}, \log g$), the other used (6550K, 3.71) for Procyon and (6550, 4.0) for θ Scl. The differential abundances for Fe I and Fe II were only 0.011 and 0.004 dex, respectively.

TABLE 2 Individual results

Spec.	N	θ Scl		Procyon		Difference		
		Ab	Err	Ab	Err	Val.	Err	Ref.
C I	7	-3.608	0.087	-3.528	0.052	-0.080	0.041	1,3
N I	3	-4.204	0.047	-3.982	0.078	-0.222	0.036	1
O I	4	-3.195	0.060	-3.201	0.056	0.006	0.067	1
Na I	4	-5.915	0.064	-5.771	0.059	-0.144	0.036	1
Mg I	3	-4.557	0.130	-4.563	0.090	0.006	0.055	1,2
Al I	2	-5.726	0.160	-5.616	0.134	-0.110	0.026	1,2,3
Si I	9	-4.490	0.069	-4.414	0.080	-0.076	0.027	1,2,3
S I	3	-4.980	0.013	-4.947	0.022	-0.033	0.017	5
Ca I	3	-5.820	0.024	-5.909	0.019	0.089	0.036	1,2
Sc II	3	-9.107	0.067	-9.051	0.074	-0.056	0.052	1,20
Ti I	13	-7.176	0.027	-7.155	0.043	-0.021	0.019	1,6
Ti II	9	-7.126	0.103	-7.163	0.094	0.037	0.020	1,2,7
V I	7	-8.297	0.029	-8.227	0.017	-0.070	0.021	1
V II	2	-8.368	0.007	-8.395	0.000	0.027	0.007	10,11
Cr I	11	-6.567	0.030	-6.576	0.036	0.009	0.015	1,2,21
Cr II	2	-6.427	0.119	-6.420	0.070	-0.007	0.050	8
Mn I	6	-6.732	0.074	-6.724	0.090	-0.008	0.017	1,2
Fe I	12	-4.699	0.020	-4.673	0.018	-0.026	0.010	1,4
Fe II	13	-4.691	0.034	-4.675	0.036	-0.016	0.008	1,4
Co I	6	-7.068	0.154	-7.026	0.141	-0.042	0.014	1,2
Ni I	21	-5.961	0.020	-5.918	0.020	-0.043	0.013	1,9
Cu I	2	-8.130	0.019	-8.016	0.022	-0.114	0.004	1,2
Zn I	1	-7.453		-7.427		-0.026		1
Y II	6	-9.904	0.054	-9.914	0.072	0.010	0.021	1,12
Zr II	2	-9.370	0.040	-9.476	0.016	0.106	0.055	13,14
Ba II	2	-9.899	0.045	-10.086	0.040	0.187	0.005	1
La II	4	-10.993	0.124	-11.207	0.121	0.214	0.008	16
Ce II	3	-10.402	0.056	-10.510	0.063	0.108	0.075	15
Nd II	5	-10.457	-0.065	-10.654	0.080	0.188	0.027	17
Sm II	3	-11.071	0.054	-11.226	0.087	0.155	0.035	18
Eu II	1	-11.521		-11.547		0.026		1,2
Gd II	2	-10.482	0.126	-10.610	0.190	0.127	0.065	19

1 NIST, Kramida et al (2019); 2 Ryabchikova et al. (2015); 3 Laverick et al. (2019); 4 solar gf; 5 Zatsarinny & Bartschat (2006); 6 Lawler et al. (2013); 7 Wood et al. (2013); 8 Bouazza et al. (2018); 9 Ruczkowski, Elantkowska, & Dembezyński (2017); 10 Biemont et al. (1989); 11 Brewer et al (2016); 12 Palmeri et al. (2017); 13 Ljung et al. (2006); 14 Quinet, Bouazza & Palmeri (2015); 15 Lawler et al. (2009); 16 Lawler et al. (2001)) 17 Den Hartog et al. (2003); 18 Lawler et al. (2006); 19 Den Hartog et al. (2006); 20 Lawler & Dakin (1989); 21 Sobeck, Lawler & Sneden 2007)

To test the sensitivity of the method to the assumed effective temperature, we retain the parameters T_e and $\log(g)$ for Procyon, and use a temperature 100K lower for θ Scl: $T_e = 6425K$. To ensure equal abundances for Fe I and II we use $\log(g) = 4.16$. The resulting differences, θ Scl minus Procyon then change from the values of Tab. 2, to -0.078 for Fe Iánd -0.063 for Fe II. The change in the differences is a significant 0.05 dex.

NLTE corrections were available for a number of our lines from the web site at the Max Planck Institute [3] (Bergemann & Nordlander 2014). The differential corrections were generally quite small (≤ 0.01 dex). For Ti I and Cr I, average corrections were +0.01 and +0.02 dex, respectively, discernable on a

[3] nlte.mpia.de

TABLE 3 Sample data table for individual analyzed lines

Spectrum	λ Å	W_λ mÅ	log (gf)	χ eV	log (El/N_{tot})
C I	4817.373	8.7	-3.080	7.480	-3.317
C I	5023.841	15.8	-2.210	7.950	-3.531
C I	5551.579	7.0	-1.900	8.640	-3.690
...	...	...	...	...	...
Na I	4497.657	19.0	-1.574	2.100	-5.773
Na I	4751.822	9.6	-2.078	2.100	-5.617
Na I	5148.838	5.6	-2.044	2.100	-5.905
...	...	...	...	...	...

A machine-readable version of the complete table is available at the CDS.

graph of our results (Fig. 1), but too small to affect the overall conclusions.

A more important source of error arises from the measurement of the equivalent widths. ARES provides an error estimate, ΔW, for each line (Sousa et al. 2015). We used a sample of 194 Fe I lines in Procyon between 3.06 and 20 mÅ. When a line is partially blended or has close neighbors, ARES will model the region, and it gives the number of lines taken into account in determining the equivalent width of an individual line. We took cases where there were no or at most one blending line. Then, the average value of $\Delta W/W$ is 0.0966. We conclude that a typical equivalent width could be $W \pm 0.0966W$, or roughly $\log(W \pm \Delta W) = \log(W) \pm 0.04$. We take this ΔW to be the standard deviation of the ARES $\log(W)$'s, and compare them with the standard deviations of our logarithmic abundances. The assumption here is that for weak lines, the abundances are proportional to the equivalent widths.

We thus compare this (0.04 dex) standard deviation with estimates of the standard deviation of calculated abundances. We used variances in the differential abundances for 12 Fe I lines and 21 Ni I lines (Tab. 2), taking them to be representative. Here the variances are $\sqrt{N}$ times the standard errors in the penultimate column of Tab. 2. We obtain 0.033 dex for the 12 Fe I lines and 0.063 for the 21 Ni I lines. These are of the same order as the 0.04 dex we derived for the ARES measurements. This is the basis of our belief that the major source of uncertainty in our abundances is the $\log(W)$ measurements. Examination of line-by-line fits and measurements by ARES leads us to conclude that such errors arise as a result of both noise in the spectra and differences in the normalization of the two spectra, and not from the ARES technique itself.
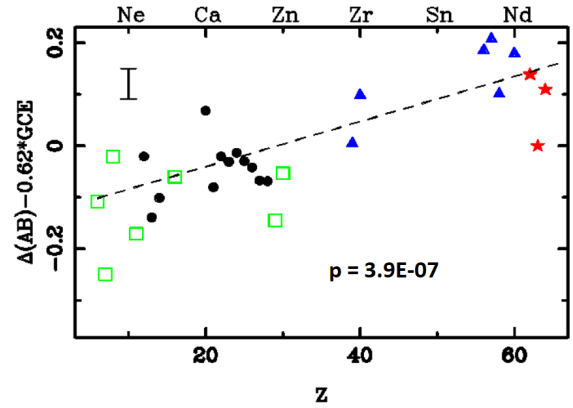

FIGURE 1 Differential logarithmic abundances (θ Scl minus Procyon) vs. atomic number Z, with corrections for GCE using an age difference of 0.62 Gyr. The vertical bar has a length of twice the average standard error (Col 8 of Tab. 2). The dashed line is $\Delta(AB) - 0.62 \cdot GCE = 4.38 \cdot 10^{-3}Z - 0.128$. Green squares are volatile elements C, N, O, Na, S, Cu, and Zn. Blue triangles are elements with a dominant s-process contribution, while red stars have a dominant r-process contribution.

6 | ABUNDANCE TRENDS

When the differential abundances of θ Scl minus Procyon are plotted versus atomic number, a highly significant relation emerges. We use Tab. 3 of BD18 to see if galactic chemical evolution (GCE) could account for that correlation. While that table is for the evolution of [El/Fe], the correction to our [El/H] for a relatively short time interval is negligible. We take 0.62 Gyr as a representative age difference based on the 2D linear interpolated values of David & Hillenbrand (2015) who give 1.48 and 2.10 Gyr for the ages of θ Scl and Procyon, respectively. A slightly smaller age difference (0.30 Gyr) results from using their 1D model (most probable) values, but differences in the range of 0 to $\sim$ 4 Gyr based on 68% confidence limits cannot be ruled out.

We subtract from each differential abundance an amount $m\Delta t$, where m is the slope of the BD18 GCE relation for each element, and Δt the difference in the ages of Procyon and θ Scl. The result is shown in Fig. 1. For convenience, we refer to the differential abundance as $\Delta(AB)$, rather than [El/H] since the latter is traditionally used for abundance differences with the Sun. Thus, $\Delta(AB) = [El/H]_{\theta\text{Scl}} - [El/H]_{\text{Procyon}}$

A linear least-squares fit to the data of Fig. 1 is indicated by the dashed line: $\Delta(AB) = 4.38 \cdot 10^{-3}Z - 0.128$. We shall refer to the coefficient $4.38 \cdot 10^{-3}$ as the "overall slope" to avoid confusion with other local slopes to be mentioned below. The fit has a Pearson correlation coefficient of 0.7849 for 28 points. The
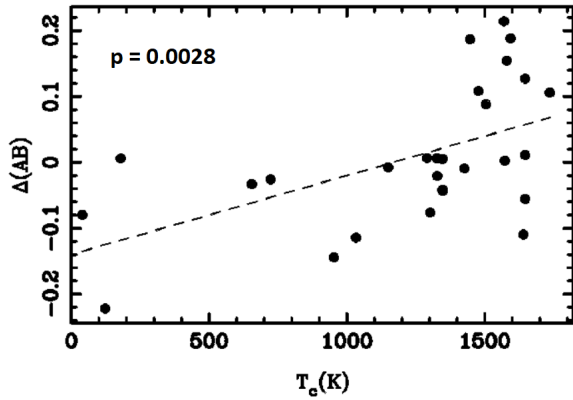
FIGURE 2 Differential abundances vs. Condensation temperature. The dashed line has the equation $\Delta(\text{Ab}) = 1.20 \cdot 10^{-4} Z - 0.140$.

corresponding probability that the relation arises by chance is $\sim 3.9 \cdot 10^{-7}$.

The overall slopes of plots like that of Fig. 1 for stars of the BD18 sample are well correlated with age (see Sec. 7, Spina et al. 2018), though there is considerable scatter. Only the youngest stars in the BD18 sample (0.5-0.6 Gyr) have slopes as large as $4.38 \cdot 10^{-3}$, and in this case the age difference of these stars with the Sun is some 4 Gyr. It is unlikely that Fig. 1 for our stars, whose probable age difference is less than ~ 1 Gyr, has its slope solely as a result of GCE. By the same token, given the uncertainties of the age estimates and the scatter in the relation between slope and age, we cannot completely exclude some contributions from GCE.

In Fig. 2, we compare our differential abundances, $\Delta(\text{Ab})$, with the 50% condensation temperature, T_c (Lodders 2003). The small correction for GCE has not been made for this plot. The probability that this plot arises by chance is 0.0028. One can make a case, though not a strong one, for the relevance of temperature-dependent condensation. Similar plots have been made by many authors in connection with solar twins (Nissen & Gustafsson 2018). Much tighter correlations are shown by Meléndez et al. (2009).

Similar trends with T_c are found in a wide variety of astronomical sources from the interstellar medium (ISM, Jenkins 2003), λ Boo stars (Heiter 2002), Post-AGB stars (Van Winckel 2003), Herbig Ae/Be stars (Folsom et al. 2012), and solar twins (Meléndez 2009). The first ionization potential effects (FIP, Laming 2015) observed in the solar and stellar coronae separate elements such as C, N, and O from heavier, iron-group elements. These chemical anomalies cover a wide range of magnitudes, from several dex in the ISM to a few hundredths of a dex in the Sun vs. solar twins. They also occur in
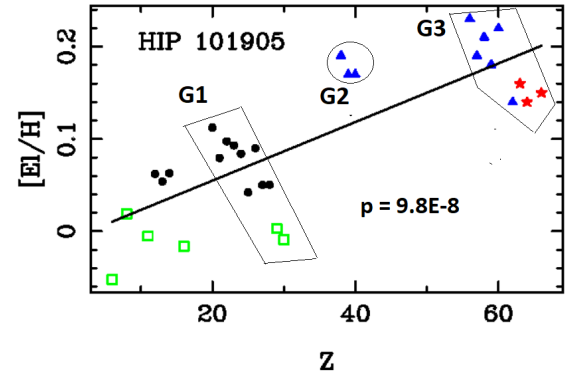

FIGURE 3 Differential abundances for HIP 101905 vs. Z showing characteristic trends and groupings of a major portion of the BD18 stars. The age of HIP 101905 is estimated to be 1.2 Gyr. The solid line has the equation: $[El/H] = 3.18 \cdot 10^{-3} Z - 0.0088$. Symbols are as in Fig. 1 .

a wide variety of astronomical settings. It is not surprising that the observed abundance patterns are variegated.

Ample discussion exists in the literature of possible scenarios that might explain such observations. These range from consequences of terrestrial planet formation to accretion of differentiated interstellar material. We refer to Nissen & Gustafsson (2018, see Sec. 4), RAM14, and other cited papers for details.

7 | ABUNDANCE PATTERNS IN THE BEDELL SAMPLE

We had expected that the differential abundances of θ Scl vs. Procyon to be random, as the stars were so similar in spectral type and population. The structure displayed in Fig. 1 led us to examine other differential results.

BD18 published precision differential abundance results for 79 solar-type stars. The focus of that and larger studies by Delgado Mena et al. (2019) or Brewer et al. (2016) primarily on the element to element abundance variations. However, the coverage of Z in the latter studies was not as complete as BD18, so we do not discuss them further here.

Our plots vs. Z display the collective behavior of numerous elements. We find a variety of patterns, many of which resemble our Fig. 1. Fig. 3 is an example of one such plot for 30 elements, carbon through dysprosium. Of BD18's 79-star sample, 35 stars show overall linear fits that are significant at the ≤ 0.01 probability level. The overall slope of those fits correlate well with age. The "local" groups G1 and G3 have significant negative slopes. G1 consists of Ca ($Z=20$) through
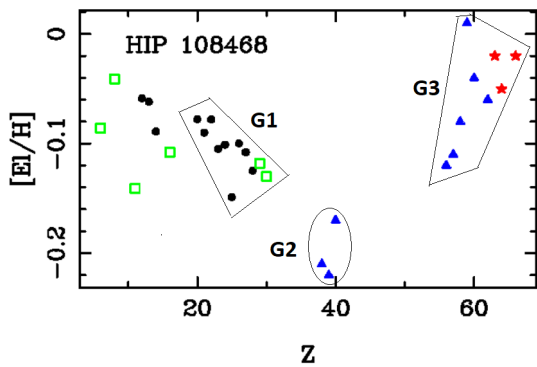
FIGURE 4 Differential abundances for the 7.4 Gyr star HIP 108468 vs. Z, illustrating the second major differential abundance pattern of the BD18 stars. Symbols are as in Fig. 1 .

Zn (Z=30), of the first long period of the Periodic Table. A straight-line fit with significance ≤ 0.01 can be obtained for the G1 points for about a third of the BD18 sample. G1 remains a coherent configuration even in some stars where the overall slope is no longer well defined, as is typical for many of the older stars. Note that G1 consists of a sequence of elements with decreasing T_c and FIP.

Roughly a third of BD18's older stars have "V-like" shapes, due to the drop of the G2 group, as shown in Fig. 4 . Note that G3 has rotated, and now has a positive slope. This positive slope is characteristic of older stars, and contributes to the V-like pattern.

8 | SUMMARY

The technique of precision differential abundances has been applied to the closely similar F-stars Procyon and θ Scl. A plot of abundance differences in the sense θ Scl minus Procyon against atomic number Z shows a highly significant positive slope and a distinct non-random pattern. This trend is unlikely to be due solely to Galactic chemical evolution. Similar patterns are found among solar-type stars in the survey of BD18, where nearly half of the 79 stars included in that sample display statistically significant overall fits, the (positive) slopes of which are correlated with age. Older stars of the BD18 collection often display markedly different patterns of differential abundance as a function of Z. A full description of the patterns and correlations within the BD18 sample will be presented in a forthcoming paper. Differential abundances for θ Scl and Procyon appear to be only weakly correlated with condensation temperature.
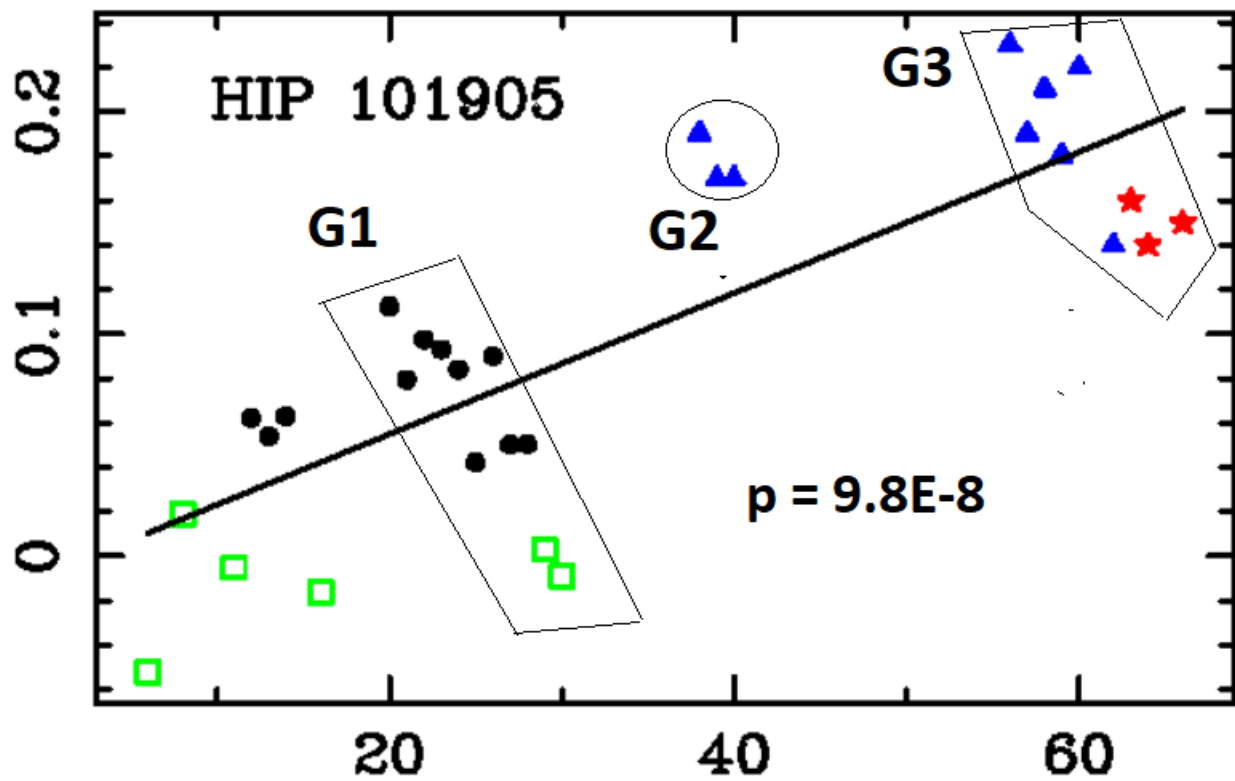
REFERENCES

Allende Prieto, C., Asplund, M., Garcia López, R. J. & Lambert, D. L. 2002, ApJ, 567, 544

Aller, L. H. 1963, Astrophysics: The Atmospheres of the Sun and Stars, (New York: Ronald Press Co.)

Asplund, M., Grevesse, N., Sauval, J. & Scott, P. 2009, ARA&A, 47, 481

Bagnulo, S., Jehin, E., Ledoux, R. et al. 2003, ESO Messenger, 114, 10

Battistini, C. & Bensby, T. 2015, A&A, 577, A9

Bedell, M., Meléndez, J., Bean, J. L. et al. 2014, ApJ, 795, 23

Bedell, M., Bean, J. L., Meléndez, J., et al. 2018, ApJ, 865, 68 (BD18)

Bergemann, M. & Nordlander, T. 2014, in Determination of Atmospheric Parameters of B-, A-, F-, and G-Type Stars, eds. E. Niemczura, B. Smalley & W. Pych (Cham: Springer), p. 169

Biémont, E., Grevesse, N., Faires, L. M., et al. 1989, A&A, 209, 391

Bouazza, S., Palmeri, P. & Quinet, P. 2018, At. Data Nucl. Data Tables, 120, 338

Brewer, J. M., Fischer, D. A., Valenti, J. A. et al. 2016, ApJS, 225, 32

Cowley, C. R., Hubrig, S. & Przybilla, N. 2014, MNRAS, 440, 2457

Cowley, C. R. & Yüce 2019, https://aas234-aas.ipostersessions.com/default.aspx?s=88-0E-2E-9F-EF-B5-F8-77-81-2D-78-25-41-DA-DC-71

David, T. J. & Hillenbrand, L. A. 2015, ApJ, 804, 146

Delgado Mena, E., Moya, A., Tsantaki, M. et al. 2019, A&A, 624, 78

Den Hartog, E. A., Lawler, J. E., Sneden, C. & Cowan, J. J. 2003, ApJS, 148, 543

Den Hartog, E. A., Lawler, J. E., Sneden, C. & Cowan, J. J. 2006, ApJS, 167, 292

Folsom, C. P., Bagnulo, S., Wade, G. A., et al. 2012, MNRAS, 422, 2072

Fuhrmann, K. & Chini, R. 2012, ApJS, 203, 30

Fuhrmann, K., Chini, R., Kaderhandt, L. & Chen, Z. 2017, ApJ, 836, 139

Gray, D. F. 2005, The Observation and Analysis of Stellar Photospheres 3rd. ed., (Cambridge: University Press)

Grevesse, N., Scott, P., Asplund, M. & Sauval, A. J. 2015, A&A, 573, 27

Heiter, U. 2002, A&A, 381, 959

Hunger, K. 1955, ZsfAp, 36, 42

Jenkins, E. B. 2003, in Origin and Evolution of the Elements, Carnegie Obs. Astrophys. Ser. 4 (Cambridge, Univ. Press, ed. A. McWilliam & M. Rauch)

Kramida, A., Ralchenko, Yu., Reader, J. et al. 2019, NIST Atomic Spectra Database (version 5.6.1), [Online], Available:http://physics.nist.gov/asd

Künzli, M., North, P., Kurucz, R. L. & Nicolet, B. 1997, A&AS, 122, 51

Kurucz, R. L., Furenlid, I., Brault, J. & Testerman, L. 1984, Solar Flux Atlas from 296 to 1300nm, NSO Atlas No. 1

Laming, J. M. 2015, LRSP, 12,2; arXiv:1504.08325

Laverick, M., Lobel, A., Royer, P., et al. 2019, A&A, 624, 60

Lawler, J. E. & Dakin, J. T. 1989, JOSA, B6, 1457

Lawler, J. E., Bonvallet, G. & Sneden, C. 2001, ApJ, 556, 452

Lawler, J. E., Den Hartog, E. A., Sneden, C. & Cowan, J. J. 2006, ApJS, 162,227

Lawler, J. E., Sneden, C., Cowan, J. J., et al. 2009, ApJS, 182, 51

Lawler, J. E., Guzman, A., Wood, M. P. et al. 2013, ApJS, 205, 11

Liebert, J., Fontaine, G., Young, P. A., et al. 2013, ApJ, 769, 7

Ljung, G., Nilsson, H., Asplund, M. & Johansson, S. 2006, A&A, 456, 1181

Lodders, K. 2003, ApJ, 591, 1220

Meléndez, J., Asplund, M., Gustafsson, B. & Yong, D. 2009, ApJL, 704, L66

Nissen, P. E. 2015, A&A, 579, 52

Nissen, P. E. & Gustafsson, B. 2018, A&AR, 26, 6

Palmeri, P., Quinet, P., Lundberg, L., et al. 2017, MNRAS, 471, 532

Quinet, P., Bouazza, S. & Palmeri, P. 2015, JQSRT, 164, 193

Ramírez, I., Meléndez, J. & Asplund, M. 2014, A&A, 561, 7 (RAM14)

Ruczkowski, J., Elantkowska, M. & Dembezyński, J. 2017, MNRAS, 464, 1127

Ryabchikova, T., Piskunov, N., Kurucz, R. L. et al. 2015, Phys. Scr. 90, 054005

Scott, P., Asplund, M., Grevesse, N., Bergemann, M. & Sauval, A. J. 2015, A&A, 573, 26

Smalley, B. 2014, in Determination of Atmospheric Parameters of B-, A-, F-, and G-Type Stars, eds. E. Niemczura, B. Smalley & W. Pych (Cham: Springer), pp 85, 111

Sobeck, J. S., Lawler, J. E. & Sneden, C. 2007, ApJ, 667, 1267

Sousa, S. G., Santos, N. C., Adibekyan, V., et al. 2015, A&A, 577, 67

Spina, L., Meléndez, J., Karakas, A. I., et al. 2018, MNRAS, 474,2580

Van Winkel, H. 2003, ARAA, 41, 391

Wood, M. P., Lawler, J. E., Sneden, C. & Cowan, J. J. 2013, ApJS, 208, 27

Zatsarinny, O. & Bartschat, K. 2006, J. Phys. 39B, 2861

☐

☐

Differential abundance analysis of Procyon and θ Sculptoris: Comparison with abundance patterns of solar-like pairs

C. R. Cowley*[1] | K. Yüce[2] | D. J. Bord[3]

[1]Department of Astronomy, University of Michigan, Ann Arbor, 1085 S. University, Michigan 48109-1107, USA

[2]Department of Astronomy and Space Sciences, Faculty of Science, University of Ankara, Ankara, TR-06100, Turkey

[3]Department of Natural Sciences, University of Michigan–Dearborn, 4901 Evergreen Road, Dearborn, MI 48128, USA

Correspondence
*C. R. Cowley Email: cowley@umich.edu

The precision differential abundance (PDA) technique is applied to the mid-F stars Procyon and θ Scl using spectra from the ESO UVESPOP library. We relate PDA patterns to endogenous processes related to condensation or to exogenous processes connected to Galactic chemical evolution (GCE). We employ one-dimensional LTE models, but emphasize the use of weaker lines ($\leq$ 20 mÅ) than are typically used in such studies. We compare our results with PDAs of solar-type stars. Abundances and PDAs are determined for 28 elements: C, N, O, Na, Mg, Al, Si, S, Ca, Sc, Ti, V, Cr, Mn, Fe, Co, Ni, Cu, Zn, Y, Zr, Ba, La, Ce, Nd, Sm, Eu, and Gd. A plot of PDAs (θ Scl minus Procyon) vs. Z shows a highly significant correlation. Moreover, local substructure of the plot for the elements Ca-Zn and neutron-addition elements is similar to that which can be found for solar twins. Our PDA vs. Z plot structural similarity to plots that can be made from the extensive work of Bedell et al. (2018). That PDA structure and substructure is clearly a function of age.

KEYWORDS:
stars:abundances, stars:solar-type, stars:individual: Procyon, stars:individual:θ Scl

Lawrence Aller (1963) discussed the differential abundance method used by mid-20th century astronomers. In it, one characterized stellar atmospheres by single, mean values of temperature and pressure. The method allowed one to avoid the use of gf-values which were often highly uncertain. This technique has been revised and updated in connection with analyses of solar twins (Melendez, et al. 2009; Nissen & Gustafsson 2018). In the modern technique, one determines basic stellar parameters and abundances from individual lines in the standard way (Gray 2005), using model atmospheres, equivalent widths and/or spectral synthesis. Differential abundances are then calculated from corresponding line pairs in the twin stars.

A primary advantage of the historical work, near independence from gf-values, is retained. The stars are chosen to have identical or nearly identical spectral types, and presumably closely comparable structures and abundances–to be "twins."

The precision of the method has revealed significant differences which may arise as a result of star formation and Galactic chemical evolution (Bedell et al. 2018, henceforth, BD18).

1 | THE STARS AND THEIR SPECTRA

Ramirez, Meléndez & Asplund (2014, henceforth RAM14) carried out an extensive study of mid and late F-star pairs. They noted that the thinness of the F-star convection zones relative to those of the well-explored solar twins would make it easier to detect abundance anomalies due, for example, to planet formation. Rather than making comparisons with the Sun, they defined standard stars from within their sample.

In the current work, we choose to compare two similar mid-F stars, slightly hotter than those of the RAM14 sample. Procyon (HD 61421) is a well-studied binary, consisting of an F5 IV-V and a white dwarf. Its composition is generally considered "indistinguishable from solar" (Liebert et al. 2013). The star,

θ Scl (HD 739), is a single-lined binary (Fuhrmann & Chini 2012, Fuhrmann et al. 2017). Its spectral type is F5 V. Contributions from the companions of either star are neglected in this study, although Procyon could be affected by pollution from its companion.

Numerous studies have given abundances for Procyon (Liebert et al. 2013). Selective abundances for θ Scl are given by Fuhrmann et al. (2017) and Battistini & Bensby (2015). The former work is not differential, while latter compares F-stars with the Sun and therefore is distinct from twin studies, which usually involve stars with effective temperatures differing by some 100K or less.

Procyon and θ Scl are in the ESO UVESPOP library (Bagnulo, et al. 2003) which provides the high-quality spectra suitable to apply the differential-twin abundance method in the F-star domain. The spectra are of comparable quality to those used used to analyze solar twins (S/N 300-700, RP 80,000).

2 | SELECTION AND MEASUREMENT OF THE LINE SPECTRA

Lines were chosen from lists from Bedell et al. (2014) and Nissen (2015), but largely from the Procyon identification list published on Cowley's web site [1]. We selected lines with no obvious blends for which the measured and Ritz wavelengths were $\leq$ 0.03Å apart. Emphasis was given to weak ($\leq$ 20 mÅ) lines (see Sec. 4). Each line was then synthesized to discern the contribution of possible blends. The decision to use a particular line was aided by a synthesis with most of the broadening turned off, e.g. no turbulent or instrumental broadening. Additional useful information came from a synthesis with the contribution from the line in question turned off.

We chose to measure equivalent widths with the automatic routine ARES (Sousa et al. 2015). The code was downloaded from S. G. Sousa's web site [2] and installed under LINUX. Our own measurements, especially those of KY, using IRAF's Gaussian fits, agreed well with those of ARES. We decided that automatic measurements would remove any influence of a personal equation from the results if the input parameters to ARES are the same for both stars.

3 | MODELS AND SOFTWARE

Atlas9 models with solar abundances were used by both CRC and KY. Solar abundances are from Asplund et al. (2009) with updates by Scott et al. (2015), and Grevesse et al. (2015). To obtain abundances from an equivalent width, KY used

WIDTH9, while CRC fit Voigt profiles (cf. Cowley et al. 2014, and references therein). We used a set of 22 Fe I and 33 Fe II lines. The equivalent widths of these iron lines ranged from 3 to 90 mÅ. The mean difference of our measurements of log(W), CRC−KY, was 0.0031 dex. These lines were used to determine the microturbulent velocity and to ensure that the abundances were independent of excitation potential.

The standard method of deriving the microturbulence is to require that the stronger lines agree in abundance with the weakest ones. However, this removes virtually all abundance information from the strongest lines. Because of this, we have based our final model parameters on 12 Fe I lines and 13 Fe II lines with equivalent widths $\lesssim$ 20mÅ (Tab. 1). Our calculations used LTE and 1-dimensional models as is still common in differential analyses (Nissen & Gustafsson 2018).

In order to choose values of $T_{\rm eff}$ and log(g) for abundance calculations, four or five models were calculated, based on initial estimates from the literature and spectral types. Fe I and II abundances (Ab) were calculated for these models. They were assumed to obey a linear relation:

$$Ab = a \cdot T_{\rm eff} + b \cdot \log(g) + c. \qquad (1)$$

The coefficients were determined separately by least squares for the reduced set of Fe I and Fe II lines (cf. Tab. 1) and then the right-hand sides of Eq. 1 were set equal to each other. This gives a linear relation between $T_{\rm eff}$ and log(g), or a line on a Kiel Diagram (Hunger 1955). This relation is also a function of the lines chosen and their gf-values (see Sec. 4).

To fix our final $T_{\rm eff}$ and log(g), we used Strömgren (Smalley 2014) and Geneva (Künzli et al. 1997) photometry, synthesis and comparison of the Balmer-line profiles, as well as the requirement that Fe I and Fe II yield the same abundance. Our adopted model for Procyon has $T_{\rm eff}$ = 6550K and log(g) = 3.9, with $v \cdot \sin(i)$ = 3.0 km/sec and a microturbulence of 2.0 km/sec. For θ Scl, these values were 6525K, 4.3, 3.0 km/sec, and 1.7 km/sec. A possible contribution from macroturbulence is included in our values of $v \cdot \sin(i)$, which were found by spectrum synthesis. These figures are in agreement with values in the literature (cf. Allende Prieto et al. 2002; Fuhrmann & Chini 2012). Uncertainties in the models and their effect on our results are discussed in Sect. 5.

4 | LINES AND TRANSITION PROBABILITIES: ABUNDANCES

4.1 | Iron

The use of very weak lines has advantages and disadvantages. Weak lines cannot be measured as accurately as stronger ones. In our experience, this is true both for lines measured "by eye" as well at those measured by ARES. Additionally, reliable

---

[1] http://www-personal.umich.edu/~cowley/procyon/wlid.html
[2] http://www.astro.up.pt/~sousasag/ares/

TABLE 1 Adopted weak Fe I and Fe II lines

Fe I			Fe II		
λ(Å)	log(gf)	Desc.	λ(Å)	log(gf)	Desc.
4808.148	-2.668	sol	4720.139	-4.570	sol
5295.312	-1.557	sol	4833.192	-4.621	sol
5386.333	-1.730	sol	4953.980	-2.680	sol
5441.339	-1.588	sol	5000.730	-4.733	sol
5491.832	-2.188	C+	5161.175	-4.203	sol
5696.089	-1.720	C+	5427.816	-1.545	sol
5855.076	-1.478	C+	5525.117	-3.970	C
6226.734	-2.098	sol	5591.360	-4.527	sol
6271.278	-2.703	C+	6113.319	-4.078	sol
6725.356	-2.212	sol	6179.390	-2.797	sol
6733.150	-1.456	sol	6239.357	-4.812	sol
6837.006	-1.687	B	6248.907	-2.427	sol
			6446.407	-1.960	V3

oscillator strengths are more difficult to find for weak features (see below). On the other hand, curve of growth effects (e.g., microturbulence and hyperfine structure) are reduced by the use of weak lines. In Cowley & Yüce (2019), we found that for a typical Fe I line with an equivalent width of 15.2 mÅ, the saturation effect weakened the line by 17%. Although with differential methods, oscillator strengths cancel, this is only true for very weak lines and for lines where the saturation effects associated with turbulence and damping are taken precisely into account.

Oscillator strengths with NIST (Kramida et al. 2019) ratings of C or better were available for a few of our weak lines. Results using values from BRASS (Laverick et al. 2019) or VALD3 (V3, Ryabchikova et al. 2015) for the remaining lines led to results with wide scatter. For those lines, we ultimately chose solar gf-values derived in this work from ARES measurements using the Kurucz solar flux atlas (Kurucz et al. 1984). The Fe lines and adopted log(gf) values are shown in Tab. 1. The column labeled "Desc" gives the NIST accuracy rating or "sol," to indicate that solar gf-values were adopted. Of 12 the Fe I lines in Tab. 1, nine overlap with Bedell et al (2014). For these lines the agreement is excellent, especially for five of the lines for which solar values were derived. None of our Fe II lines overlapped with Bedell et al (2014).

4.2 | Other elements

In order to select lines for analysis, ARES was given a list of all lines from the Procyon identification list which had a single attribute whose wavelength differed by ≤ 0.03Å. We then chose lines, with a few exceptions, having equivalent widths ≤ 20 mÅ. Of the 174 lines used for abundances, eight have

equivalent widths ≥ 20 mÅ. The largest of these was Eu II with 45.5 mÅ in Procyon. Generally, hyperfine structure was not taken into account for our weak lines, but for this line in Eu II it was approximately taken into account using the data of VALD3.

The regions near all of these lines were synthesized, as described for the iron lines. While virtually all of the lines had small blends, lines were retained unless the blends were estimated to contribute 10% or more to equivalent widths.

All of the lines judged suitable for analysis in the Procyon spectrum were adopted for θ Scl, provided there was an ARES measurement. In a few cases, lines measured by ARES for Procyon were not measured in θ Scl. Usually such lines were discarded from the analysis, but rarely, the lines were remeasured by CRC. Such measurements intercompare very well for weak lines with KY's IRAF values. The lines in question are: Nd II 5092.77, 5092.81 and Gd II 4316.04.

We consulted the bibliographic reference data of NIST (Kramida et al. 2019) to select the most recently determined oscillator strengths. Where practical, we cite original work rather than compilations (see Column 9 in Tab. 2).

Derived abundances are given in Tab. 2. The abundances are for $\log(El/N_{\rm tot}) = \log(El/H) - 0.036$. The Difference column is for (θ Scl minus Procyon). The error of the differences is calculated for the N individual line pairs for each spectrum. Data for individual lines are given in Tab. 3.

5 | ERRORS

We have listed standard errors in Tab. 2, which are smaller by $\sqrt{N}$ than standard deviations, which can readily be obtained using Tab. 2. In general, while standard errors are technically correct, standard deviations often give a more realistic estimate of the uncertainties because statistical analysis does not account for systematic errors. The present differential technique should eliminate many systematic errors, however.

The average standard error of our differential abundances (Column 8 of Tab. 2) is 0.0294 dex. Overall, we have not reached the level of accuracy, 0.01 dex, of the solar twin studies (e.g. Meléndez et al. 2009; Nissen 2015), although for a few species, including Fe I and II, our standard errors are of the order of 0.01 dex.

Uncertainties in the model parameters introduce some error. Cowley & Yüce (2019, see Series 3 slide 3) gave results of a differential analysis for two sets of parameters describing Procyon and θ Scl. One set of results for Fe I and Fe II used the current parameters ($T_{\rm eff}, \log g$), the other used (6550K, 3.71) for Procyon and (6550, 4.0) for θ Scl. The differential abundances for Fe I and Fe II were only 0.011 and 0.004 dex, respectively.

TABLE 2 Individual results

Spec.	N	θ Scl Ab	θ Scl Err	Procyon Ab	Procyon Err	Difference Val.	Difference Err	Ref.
C I	7	-3.608	0.087	-3.528	0.052	-0.080	0.041	1,3
N I	3	-4.204	0.047	-3.982	0.078	-0.222	0.036	1
O I	4	-3.195	0.060	-3.201	0.056	0.006	0.067	1
Na I	4	-5.915	0.064	-5.771	0.059	-0.144	0.036	1
Mg I	3	-4.557	0.130	-4.563	0.090	0.006	0.055	1,2
Al I	2	-5.726	0.160	-5.616	0.134	-0.110	0.026	1,2,3
Si I	9	-4.490	0.069	-4.414	0.080	-0.076	0.027	1,2,3
S I	3	-4.980	0.013	-4.947	0.022	-0.033	0.017	5
Ca I	3	-5.820	0.024	-5.909	0.019	0.089	0.036	1,2
Sc II	3	-9.107	0.067	-9.051	0.074	-0.056	0.052	1,20
Ti I	13	-7.176	0.027	-7.155	0.043	-0.021	0.019	1,6
Ti II	9	-7.126	0.103	-7.163	0.094	0.037	0.020	1,2,7
V I	7	-8.297	0.029	-8.227	0.017	-0.070	0.021	1
V II	2	-8.368	0.007	-8.395	0.000	0.027	0.007	10,11
Cr I	11	-6.567	0.030	-6.576	0.036	0.009	0.015	1,2,21
Cr II	2	-6.427	0.119	-6.420	0.070	-0.007	0.050	8
Mn I	6	-6.732	0.074	-6.724	0.090	-0.008	0.017	1,2
Fe I	12	-4.699	0.020	-4.673	0.018	-0.026	0.010	1,4
Fe II	13	-4.691	0.034	-4.675	0.036	-0.016	0.008	1,4
Co I	6	-7.068	0.154	-7.026	0.141	-0.042	0.014	1,2
Ni I	21	-5.961	0.020	-5.918	0.020	-0.043	0.013	1,9
Cu I	2	-8.130	0.019	-8.016	0.022	-0.114	0.004	1,2
Zn I	1	-7.453		-7.427		-0.026		1
Y II	6	-9.904	0.054	-9.914	0.072	0.010	0.021	1,12
Zr II	2	-9.370	0.040	-9.476	0.016	0.106	0.055	13,14
Ba II	2	-9.899	0.045	-10.086	0.040	0.187	0.005	1
La II	4	-10.993	0.124	-11.207	0.121	0.214	0.008	16
Ce II	3	-10.402	0.056	-10.510	0.063	0.108	0.075	15
Nd II	5	-10.457	-0.065	-10.654	0.080	0.188	0.027	17
Sm II	3	-11.071	0.054	-11.226	0.087	0.155	0.035	18
Eu II	1	-11.521		-11.547		0.026	1,2	
Gd II	2	-10.482	0.126	-10.610	0.190	0.127	0.065	19

1 NIST, Kramida et al (2019); 2 Ryabchikova et al. (2015); 3 Laverick et al. (2019); 4 solar gf; 5 Zatsarinny & Bartschat (2006); 6 Lawler et al. (2013); 7 Wood et al. (2013); 8 Bouazza et al. (2018); 9 Ruczkowski, Elantkowska, & Dembezyński (2017); 10 Biemont et al. (1989); 11 Brewer et al (2016); 12 Palmeri et al. (2017); 13 Ljung et al. (2006); 14 Quinet, Bouazza & Palmeri (2015); 15 Lawler et al. (2009); 16 Lawler et al. (2001)) 17 Den Hartog et al. (2003); 18 Lawler et al. (2006); 19 Den Hartog et al. (2006); 20 Lawler & Dakin (1989); 21 Sobeck, Lawler & Sneden 2007)

To test the sensitivity of the method to the assumed effective temperature, we retain the parameters T_e and $\log(g)$ for Procyon, and use a temperature 100K lower for θ Scl: $T_e = 6425K$. To ensure equal abundances for Fe I and II we use $\log(g) = 4.16$. The resulting differences, θ Scl minus Procyon then change from the values of Tab. 2, to -0.078 for Fe I and -0.063 for Fe II. The change in the differences is a significant 0.05 dex.

NLTE corrections were available for a number of our lines from the web site at the Max Planck Institute [3] (Bergemann & Nordlander 2014). The differential corrections were generally quite small (≤ 0.01 dex). For Ti I and Cr I, average corrections were +0.01 and +0.02 dex, respectively, discernable on a

---

[3]nlte.mpia.de

TABLE 3 Sample data table for individual analyzed lines

Spectrum	λ Å	W_λ mÅ	$\log$ (gf)	χ eV	$\log$ (El/N_{tot})
C I	4817.373	8.7	-3.080	7.480	-3.317
C I	5023.841	15.8	-2.210	7.950	-3.531
C I	5551.579	7.0	-1.900	8.640	-3.690
...	...	...	...	...	...
Na I	4497.657	19.0	-1.574	2.100	-5.773
Na I	4751.822	9.6	-2.078	2.100	-5.617
Na I	5148.838	5.6	-2.044	2.100	-5.905
...	...	...	...	...	...

A machine-readable version of the complete table is available at the CDS.

graph of our results (Fig. 1), but too small to affect the overall conclusions.

A more important source of error arises from the measurement of the equivalent widths. ARES provides an error estimate, ΔW, for each line (Sousa et al. 2015). We used a sample of 194 Fe I lines in Procyon between 3.06 and 20 mÅ. When a line is partially blended or has close neighbors, ARES will model the region, and it gives the number of lines taken into account in determining the equivalent width of an individual line. We took cases where there were no or at most one blending line. Then, the average value of $\Delta W/W$ is 0.0966. We conclude that a typical equivalent width could be $W \pm 0.0966W$, or roughly $\log(W \pm \Delta W) = \log(W) \pm 0.04$. We take this ΔW to be the standard deviation of the ARES $\log(W)$'s, and compare them with the standard deviations of our logarithmic abundances. The assumption here is that for weak lines, the abundances are proportional to the equivalent widths.

We thus compare this (0.04 dex) standard deviation with estimates of the standard deviation of calculated abundances. We used variances in the differential abundances for 12 Fe I lines and 21 Ni I lines (Tab. 2), taking them to be representative. Here the variances are $\sqrt{N}$ times the standard errors in the penultimate column of Tab. 2. We obtain 0.033 dex for the 12 Fe I lines and 0.063 for the 21 Ni I lines. These are of the same order as the 0.04 dex we derived for the ARES measurements. This is the basis of our belief that the major source of uncertainty in our abundances is the $\log(W)$ measurements. Examination of line-by-line fits and measurements by ARES leads us to conclude that such errors arise as a result of both noise in the spectra and differences in the normalization of the two spectra, and not from the ARES technique itself.
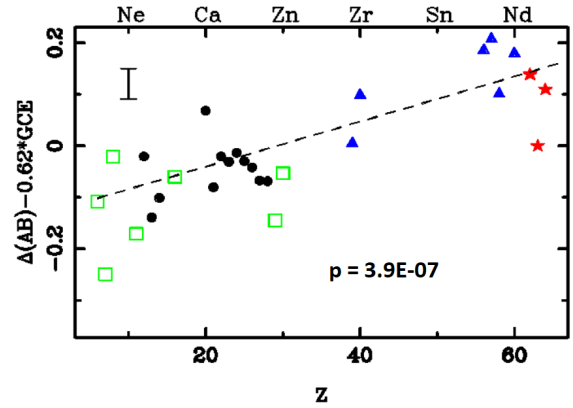

FIGURE 1 Differential logarithmic abundances (θ Scl minus Procyon) vs. atomic number Z, with corrections for GCE using an age difference of 0.62 Gyr. The vertical bar has a length of twice the average standard error (Col 8 of Tab. 2). The dashed line is $\Delta(AB) - 0.62 \cdot GCE = 4.38 \cdot 10^{-3}Z - 0.128$. Green squares are volatile elements C, N, O, Na, S, Cu, and Zn. Blue triangles are elements with a dominant s-process contribution, while red stars have a dominant r-process contribution.

6 | ABUNDANCE TRENDS

When the differential abundances of θ Scl minus Procyon are plotted versus atomic number, a highly significant relation emerges. We use Tab. 3 of BD18 to see if galactic chemical evolution (GCE) could account for that correlation. While that table is for the evolution of [El/Fe], the correction to our [El/H] for a relatively short time interval is negligible. We take 0.62 Gyr as a representative age difference based on the 2D linear interpolated values of David & Hillenbrand (2015) who give 1.48 and 2.10 Gyr for the ages of θ Scl and Procyon, respectively. A slightly smaller age difference (0.30 Gyr) results from using their 1D model (most probable) values, but differences in the range of 0 to $\sim$ 4 Gyr based on 68% confidence limits cannot be ruled out.

We subtract from each differential abundance an amount $m\Delta t$, where m is the slope of the BD18 GCE relation for each element, and Δt the difference in the ages of Procyon and θ Scl. The result is shown in Fig. 1. For convenience, we refer to the differential abundance as $\Delta(AB)$, rather than [El/H] since the latter is traditionally used for abundance differences with the Sun. Thus, $\Delta(AB) = [El/H]_{\theta\text{Scl}} - [El/H]_{\text{Procyon}}$

A linear least-squares fit to the data of Fig. 1 is indicated by the dashed line: $\Delta(AB) = 4.38 \cdot 10^{-3}Z - 0.128$. We shall refer to the coefficient $4.38 \cdot 10^{-3}$ as the "overall slope" to avoid confusion with other local slopes to be mentioned below. The fit has a Pearson correlation coefficient of 0.7849 for 28 points. The
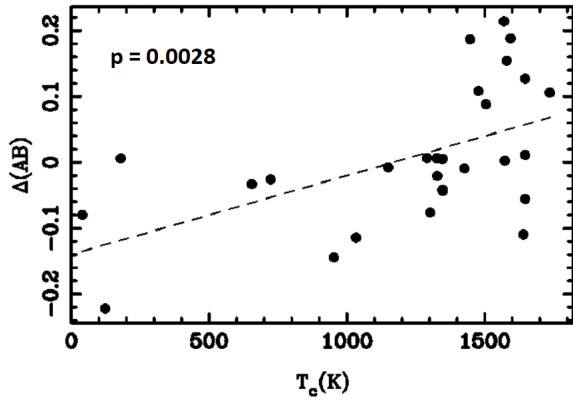
FIGURE 2 Differential abundances vs. Condensation temperature. The dashed line has the equation $\Delta(\text{Ab}) = 1.20 \cdot 10^{-4}Z - 0.140$.

corresponding probability that the relation arises by chance is $\sim 3.9 \cdot 10^{-7}$.

The overall slopes of plots like that of Fig. 1 for stars of the BD18 sample are well correlated with age (see Sec. 7, Spina et al. 2018), though there is considerable scatter. Only the youngest stars in the BD18 sample (0.5-0.6 Gyr) have slopes as large as $4.38 \cdot 10^{-3}$, and in this case the age difference of these stars with the Sun is some 4 Gyr. It is unlikely that Fig. 1 for our stars, whose probable age difference is less than ~ 1 Gyr, has its slope solely as a result of GCE. By the same token, given the uncertainties of the age estimates and the scatter in the relation between slope and age, we cannot completely exclude some contributions from GCE.

In Fig. 2, we compare our differential abundances, $\Delta(\text{Ab})$, with the 50% condensation temperature, T_c (Lodders 2003). The small correction for GCE has not been made for this plot. The probability that this plot arises by chance is 0.0028. One can make a case, though not a strong one, for the relevance of temperature-dependent condensation. Similar plots have been made by many authors in connection with solar twins (Nissen & Gustafsson 2018). Much tighter correlations are shown by Meléndez et al. (2009).

Similar trends with T_c are found in a wide variety of astronomical sources from the interstellar medium (ISM, Jenkins 2003), λ Boo stars (Heiter 2002), Post-AGB stars (Van Winckel 2003), Herbig Ae/Be stars (Folsom et al. 2012), and solar twins (Meléndez 2009). The first ionization potential effects (FIP, Laming 2015) observed in the solar and stellar coronae separate elements such as C, N, and O from heavier, iron-group elements. These chemical anomalies cover a wide range of magnitudes, from several dex in the ISM to a few hundredths of a dex in the Sun vs. solar twins. They also occur in
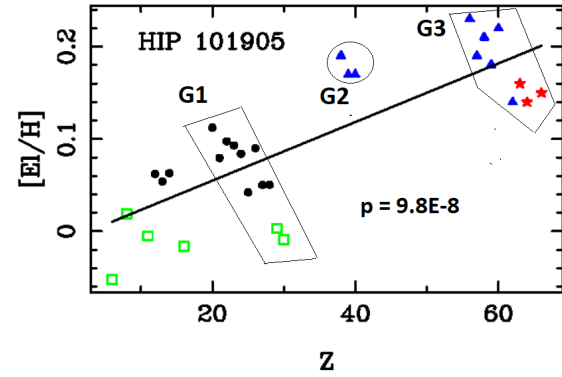

FIGURE 3 Differential abundances for HIP 101905 vs. Z showing characteristic trends and groupings of a major portion of the BD18 stars. The age of HIP 101905 is estimated to be 1.2 Gyr. The solid line has the equation: $[El/H] = 3.18 \cdot 10^{-3}Z - 0.0088$. Symbols are as in Fig. 1 .

a wide variety of astronomical settings. It is not surprising that the observed abundance patterns are variegated.

Ample discussion exists in the literature of possible scenarios that might explain such observations. These range from consequences of terrestrial planet formation to accretion of differentiated interstellar material. We refer to Nissen & Gustafsson (2018, see Sec. 4), RAM14, and other cited papers for details.

7 | ABUNDANCE PATTERNS IN THE BEDELL SAMPLE

We had expected that the differential abundances of θ Scl vs. Procyon to be random, as the stars were so similar in spectral type and population. The structure displayed in Fig. 1 led us to examine other differential results.

BD18 published precision differential abundance results for 79 solar-type stars. The focus of that and larger studies by Delgado Mena et al. (2019) or Brewer et al. (2016) primarily on the element to element abundance variations. However, the coverage of Z in the latter studies was not as complete as BD18, so we do not discuss them further here.

Our plots vs. Z display the collective behavior of numerous elements. We find a variety of patterns, many of which resemble our Fig. 1. Fig. 3 is an example of one such plot for 30 elements, carbon through dysprosium. Of BD18's 79-star sample, 35 stars show overall linear fits that are significant at the ≤ 0.01 probability level. The overall slope of those fits correlate well with age. The "local" groups G1 and G3 have significant negative slopes. G1 consists of Ca ($Z=20$) through
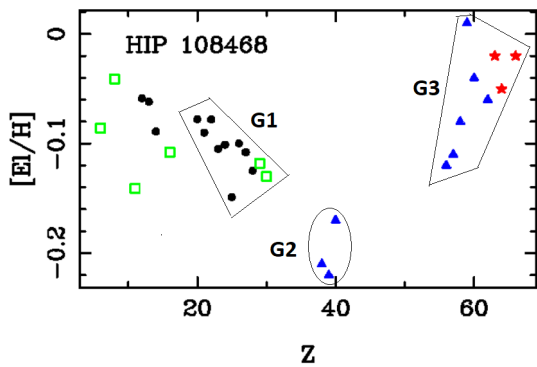
FIGURE 4 Differential abundances for the 7.4 Gyr star HIP 108468 vs. Z, illustrating the second major differential abundance pattern of the BD18 stars. Symbols are as in Fig. 1 .

Zn (Z=30), of the first long period of the Periodic Table. A straight-line fit with significance ≤ 0.01 can be obtained for the G1 points for about a third of the BD18 sample. G1 remains a coherent configuration even in some stars where the overall slope is no longer well defined, as is typical for many of the older stars. Note that G1 consists of a sequence of elements with decreasing T_c and FIP.

Roughly a third of BD18's older stars have "V-like" shapes, due to the drop of the G2 group, as shown in Fig. 4 . Note that G3 has rotated, and now has a positive slope. This positive slope is characteristic of older stars, and contributes to the V-like pattern.

8 | SUMMARY

The technique of precision differential abundances has been applied to the closely similar F-stars Procyon and θ Scl. A plot of abundance differences in the sense θ Scl minus Procyon against atomic number Z shows a highly significant positive slope and a distinct non-random pattern. This trend is unlikely to be due solely to Galactic chemical evolution. Similar patterns are found among solar-type stars in the survey of BD18, where nearly half of the 79 stars included in that sample display statistically significant overall fits, the (positive) slopes of which are correlated with age. Older stars of the BD18 collection often display markedly different patterns of differential abundance as a function of Z. A full description of the patterns and correlations within the BD18 sample will be presented in a forthcoming paper. Differential abundances for θ Scl and Procyon appear to be only weakly correlated with condensation temperature.
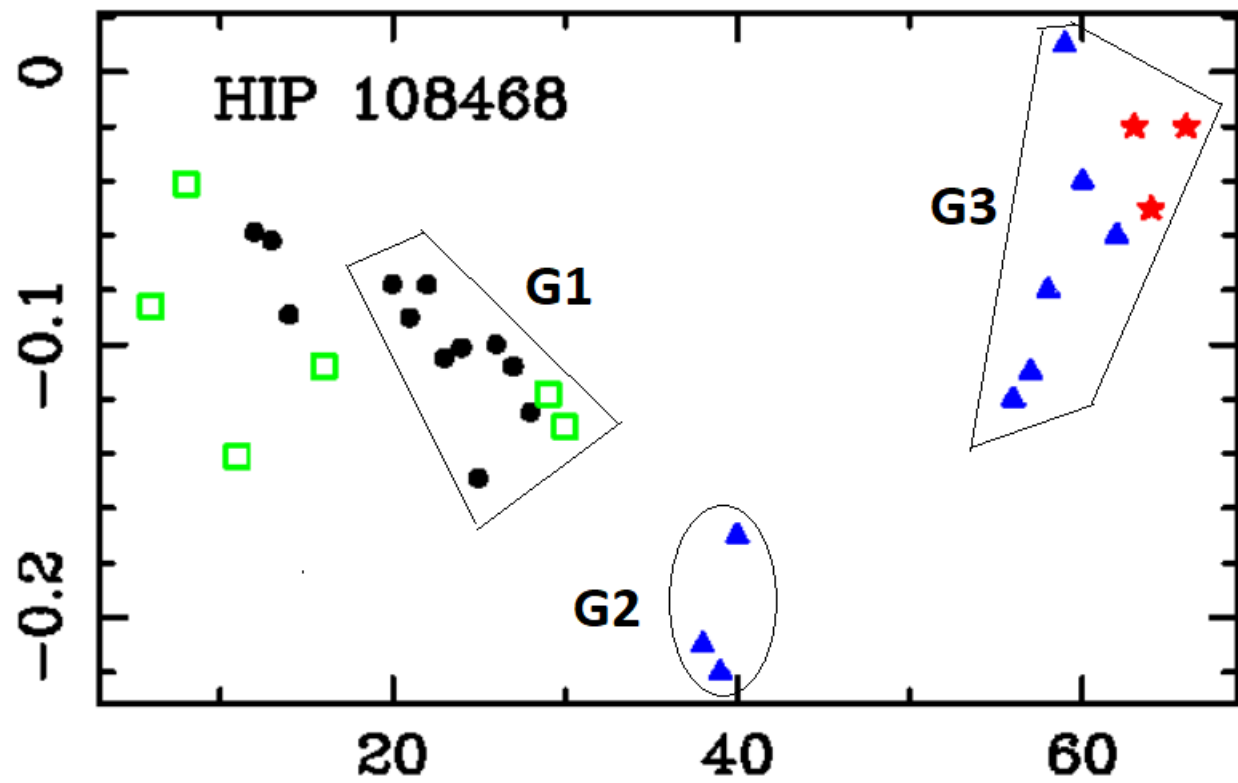
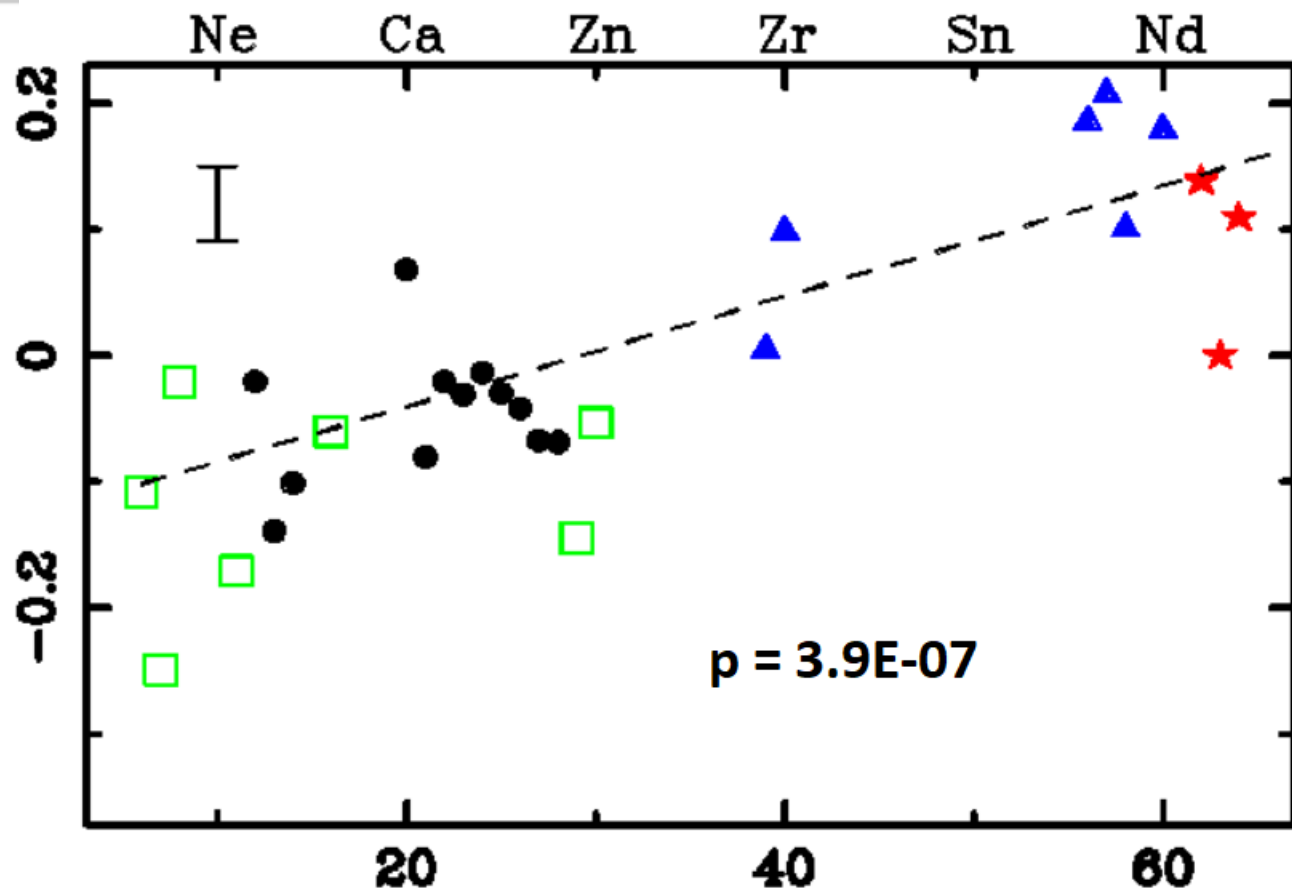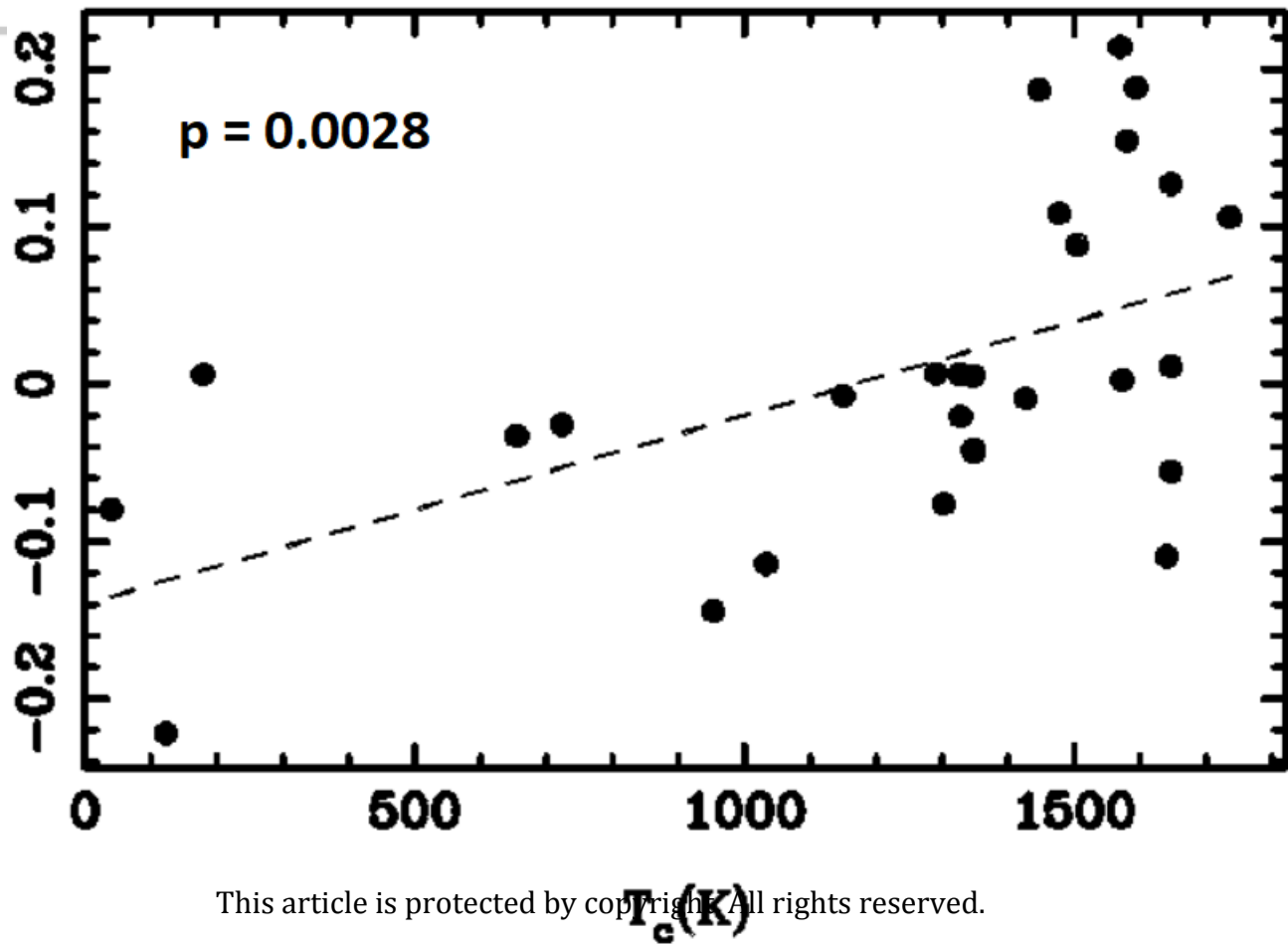# REFERENCES

Allende Prieto, C., Asplund, M., Garcia López, R. J. & Lambert, D. L. 2002, ApJ, 567, 544

Aller, L. H. 1963, Astrophysics: The Atmospheres of the Sun and Stars, (New York: Ronald Press Co.)

Asplund, M., Grevesse, N., Sauval, J. & Scott, P. 2009, ARA&A, 47, 481

Bagnulo, S., Jehin, E., Ledoux, R. et al. 2003, ESO Messenger, 114, 10

Battistini, C. & Bensby, T. 2015, A&A, 577, A9

Bedell, M., Meléndez, J., Bean, J. L. et al. 2014, ApJ, 795, 23

Bedell, M., Bean, J. L., Meléndez, J., et al. 2018, ApJ, 865, 68 (BD18)

Bergemann, M. & Nordlander, T. 2014, in Determination of Atmospheric Parameters of B-, A-, F-, and G-Type Stars, eds. E. Niemczura, B. Smalley & W. Pych (Cham: Springer), p. 169

Biémont, E., Grevesse, N., Faires, L. M., et al. 1989, A&A, 209, 391

Bouazza, S., Palmeri, P. & Quinet, P. 2018, At. Data Nucl. Data Tables, 120, 338

Brewer, J. M., Fischer, D. A., Valenti, J. A. et al. 2016, ApJS, 225, 32

Cowley, C. R., Hubrig, S. & Przybilla, N. 2014, MNRAS, 440, 2457

Cowley, C. R. & Yüce 2019, https://aas234-aas.ipostersessions.com/default.aspx?s=88-0E-2E-9F-EF-B5-F8-77-81-2D-78-25-41-DA-DC-71

David, T. J. & Hillenbrand, L. A. 2015, ApJ, 804, 146

Delgado Mena, E., Moya, A., Tsantaki, M. et al. 2019, A&A, 624, 78

Den Hartog, E. A., Lawler, J. E., Sneden, C. & Cowan, J. J. 2003, ApJS, 148, 543

Den Hartog, E. A., Lawler, J. E., Sneden, C. & Cowan, J. J. 2006, ApJS, 167, 292

Folsom, C. P., Bagnulo, S., Wade, G. A., et al. 2012, MNRAS, 422, 2072

Fuhrmann, K. & Chini, R. 2012, ApJS, 203, 30

Fuhrmann, K., Chini, R., Kaderhandt, L. & Chen, Z. 2017, ApJ, 836, 139

Gray, D. F. 2005, The Observation and Analysis of Stellar Photospheres 3rd. ed., (Cambridge: University Press)

Grevesse, N., Scott, P., Asplund, M. & Sauval, A. J. 2015, A&A, 573, 27

Heiter, U. 2002, A&A, 381, 959

Hunger, K. 1955, ZsfAp, 36, 42

Jenkins, E. B. 2003, in Origin and Evolution of the Elements, Carnegie Obs. Astrophys. Ser. 4 (Cambridge, Univ. Press, ed. A. McWilliam & M. Rauch)

Kramida, A., Ralchenko, Yu., Reader, J. et al. 2019, NIST Atomic Spectra Database (version 5.6.1), [Online], Available:http://physics.nist.gov/asd

Künzli, M., North, P., Kurucz, R. L. & Nicolet, B. 1997, A&AS, 122, 51

Kurucz, R. L., Furenlid, I., Brault, J. & Testerman, L. 1984, Solar Flux Atlas from 296 to 1300nm, NSO Atlas No. 1

Laming, J. M. 2015, LRSP, 12,2; arXiv:1504.08325

Laverick, M., Lobel, A., Royer, P., et al. 2019, A&A, 624, 60

Lawler, J. E. & Dakin, J. T. 1989, JOSA, B6, 1457

Lawler, J. E., Bonvallet, G. & Sneden, C. 2001, ApJ, 556, 452

Lawler, J. E., Den Hartog, E. A., Sneden, C. & Cowan, J. J. 2006, ApJS, 162,227

Lawler, J. E., Sneden, C., Cowan, J. J., et al. 2009, ApJS, 182, 51

Lawler, J. E., Guzman, A., Wood, M. P. et al. 2013, ApJS, 205, 11

Liebert, J., Fontaine, G., Young, P. A., et al. 2013, ApJ, 769, 7

Ljung, G., Nilsson, H., Asplund, M. & Johansson, S. 2006, A&A, 456, 1181

Lodders, K. 2003, ApJ, 591, 1220

Meléndez, J., Asplund, M., Gustafsson, B. & Yong, D. 2009, ApJL, 704, L66

Nissen, P. E. 2015, A&A, 579, 52

Nissen, P. E. & Gustafsson, B. 2018, A&AR, 26, 6

Palmeri, P., Quinet, P., Lundberg, L., et al. 2017, MNRAS, 471, 532

Quinet, P., Bouazza, S. & Palmeri, P. 2015, JQSRT, 164, 193

Ramírez, I., Meléndez, J. & Asplund, M. 2014, A&A, 561, 7 (RAM14)

Ruczkowski, J., Elantkowska, M. & Dembezyński, J. 2017, MNRAS, 464, 1127

Ryabchikova, T., Piskunov, N., Kurucz, R. L. et al. 2015, Phys. Scr. 90, 054005

Scott, P., Asplund, M., Grevesse, N., Bergemann, M. & Sauval, A. J. 2015, A&A, 573, 26

Smalley, B. 2014, in Determination of Atmospheric Parameters of B-, A-, F-, and G-Type Stars, eds. E. Niemczura, B. Smalley & W. Pych (Cham: Springer), pp 85, 111

Sobeck, J. S., Lawler, J. E. & Sneden, C. 2007, ApJ, 667, 1267

Sousa, S. G., Santos, N. C., Adibekyan, V., et al. 2015, A&A, 577, 67

Spina, L., Meléndez, J., Karakas, A. I., et al. 2018, MNRAS, 474,2580

Van Winkel, H. 2003, ARAA, 41, 391

Wood, M. P., Lawler, J. E., Sneden, C. & Cowan, J. J. 2013, ApJS, 208, 27

Zatsarinny, O. & Bartschat, K. 2006, J. Phys. 39B, 2861

☐

☐